JOURNAL OF AIRCRAFT
Vol. 37, No. 4, July–August 2000

Robust Vortex Control of a Delta Wing by Distributed Microelectromechanical-Systems Actuators

Gwo-Bin Lee*
National Cheng-Kung University, Tainan, Taiwan 701, Republic of China
Chiang Shih†
Florida A&M University and Florida State University, Tallahassee, Florida 32310
Yu-Chong Tai‡ and Thomas Tsao‡
California Institute of Technology, Pasadena, California 91125
Chang Liu§
University of Illinois at Urbana–Champaign, Urbana, Illinois 61801
and
Adam Huang¶ and Chih-Ming Ho¶
University of California, Los Angeles, Los Angeles, California 90095

Micromachined actuators have been used successfully to control leading-edge vortices of a delta wing by manipulating the thin boundary layer before flow separation. In an earlier work (Lee, G. B., Ho, C. M., Jiang, F., Liu, C., Tsao, T., and Tai, Y. C., "Distributed Flow Control by MEMS," American Society of Mechanical Engineers; International Mechanical Engineering and Exposition Nov. 1996), we demonstrated that small disturbances generated by these microactuators could alter large-scale vortex structures and consequently generate appreciable aerodynamic moments along all three axes for flight control. In the current study, we explored the possibility of independently controlling these moments. Instead of using a linearly distributed array of microactuators covering the entire leading edge as done in the previous study, we applied a shorter array of actuators located on either the forward or the rear half-section of the leading edge. Both one- and two-sided control configurations have also been investigated. Data showed that the pitching moment could be generated independently by appropriate actuation of the microactuators. To understand the interaction between the microactuators and leading-edge vortices, we conducted surface pressure distribution, direct force measurements, and flow visualization experiments. We investigated the effects of microactuators on the vortex structure, especially vortex core location. Experimental results showed that asymmetric vortex pairs were formed, which leads to the generation of significant torques in all three axes.

Nomenclature

C_l = rolling moment coefficients
C_m = pitching moment coefficients
C_n = yawing moment coefficients
C_p = pressure coefficient, $(P - P_\infty)/\frac{1}{2}\rho U^2$
c = chord length
d = characteristic length
L_v = vortex lift
P = surface pressure
P_∞ = freestream pressure
Re = Reynolds number
S = half-span
U = freestream velocity
α = angle of attack
ρ = density
θ = angular position of the actuator array measured from the bottom surface

Received 26 August 1999; revision received 21 March 2000; accepted for publication 23 March 2000.

*Assistant Professor, Department of Engineering Science. Member AIAA.
†Associate Professor, Department of Mechanical Engineering.
‡Associate Professor, Department of Electrical Engineering.
§Assistant Professor, Department of Electrical and Computer Engineering.
¶Professor, Department of Mechanical and Aerospace Engineering. AIAA Fellow.

Introduction

FLOWS over delta wings have been studied extensively in the literature.[1–5] Even at small angles of attack, a pair of spiral vortices originating from the leading edges characterize the flow on the leeward side of the wing (Fig. 1). Peckham[6] reported that leading-edge vortices could be observed at an angle of attack (AOA) as low as 2 deg for delta wings with sharp leading edges. For wings with rounded leading edges, the vortex pairs occur at higher angles of attack as a result of a delay of flow separation. Earnshaw and Lawford[7] found that these vortices start to appear at an angle of attack of 5 deg. The boundary-layer flow separating from the leading edges will form a free shear layer, which will roll up into a core of high vorticity residing above the leeward side of the wing. The vortex core grows in radius along the downstream direction, and the transverse size of the vortex is of the order of half the wing span at high AOAs. In addition to the swirl velocity component, each of the two leading-edge vortices contains an axial flow component in the central core region. As the vortex convects downstream, vorticity is continuously fed into the core region, and the circulation about the core increases. Thus, a low-pressure region will be generated by the leading-edge vortices. "Vortex lift," which is distinguished from potential lift, is created as the result of the presence of this low-pressure region. At high AOAs, the cores of leading-edge vortices on the wing tend to burst or break down.[8] Before vortex breakdown occurs, a significant portion of the total lift is attributed to the emergence of these leading-edge vortices.[9] This implies that we can generate a torque for flight control if we can break the symmetry of these two vortices.

The majority of vortex-control techniques discussed in the literature fall into five categories: a) blowing,[10–23] b) suction,[24,25]

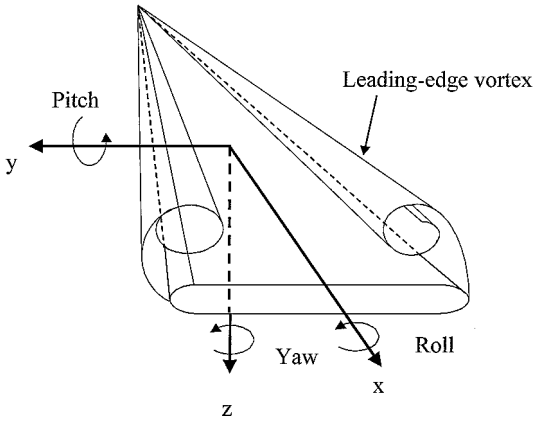

Fig. 1 Typical vortical flow over a delta wing (with round leading edges) at moderate angles of attack.

c) trailing-edge jet control,[26,27] d) large mechanical flaps,[28–32] and e) heating.[33] These approaches achieve vortex control by either altering the vorticity generation near the leading edges or manipulating the vorticity convection along the vortex core. Recently, a new delta wing vortex-control strategy using a linearly distributed array of microactuators was developed.[34,35] This actuator array, covering the entire leading edge from the apex to the trailing edge, called the AT (apex–trailing edge) actuator, has been shown to be effective in torque generation. It has been shown that if the deflection amplitude of the actuators is comparable to the boundary-layer thickness near the leading-edge separation point, it is possible to perturb the separated flow and break the symmetry of the primary vortex pair. For this purpose, microactuators with out-of-plane deflection lengths of the order of 1–2 mm have been used to control a delta wing. A significant increase in rolling, pitching, and yawing moments has been observed. It has also been found that the optimum angular location of actuators for the maximum torque generation is closely related to leading-edge flow separation.[27] On delta wings with rounded leading edges, the position of flow separation depends not only on the Reynolds number but also on the leading-edge curvature that determines the local pressure gradient. Consequently, the leading-edge flow separation line usually is not a straight line from the apex to the trailing edge. As a result, a straight array of distributed microactuators cannot match exactly with the curved separation line to produce the optimum effect. Furthermore, a partially misplaced actuator array can sometimes produce adverse effects to offset the overall control goal. In this paper, different types of distributed microactuators are used to investigate potential solutions to this problem. A shorter array of microactuators that covers only half the length from the apex to trailing edge, called the HAT (half-apex to trailing edge) actuator, was used to explore the possibility of providing more robust vortex control. Because the angular position of the HAT actuator array can be adjusted to fit more closely to the separation line on the forward (or rear) half-part of the leading edge, it is expected to generate higher torques in all three axes. Consequently, fewer actuators will be required for effective flight control, which implies a simpler hardware arrangement and less power consumption. When we installed the HAT actuator on one of the leading edges, we did destroy the symmetry of the vortex pair and produced higher rolling, pitching, and yawing moments. In addition, we also demonstrated a strategy to control the pitching moment independently by applying HAT actuators on both sides of the wing. Figure 2 presents schematically all different actuator configurations used in the paper. A detailed discussion of these results is presented in the Results and Discussion section. Currently, we are proceeding to use a large number of actuators for truly distributed control along the curved separation line.

In order to investigate the interaction between the microactuators and the vortices, a fundamental understanding of the flowfield is essential. In light of this, we conducted a series of aerodynamic tests, including surface pressure, direct force measurements, and flow visualization experiments, with and without flow control. The objective of this work is to investigate how the vortex structure is

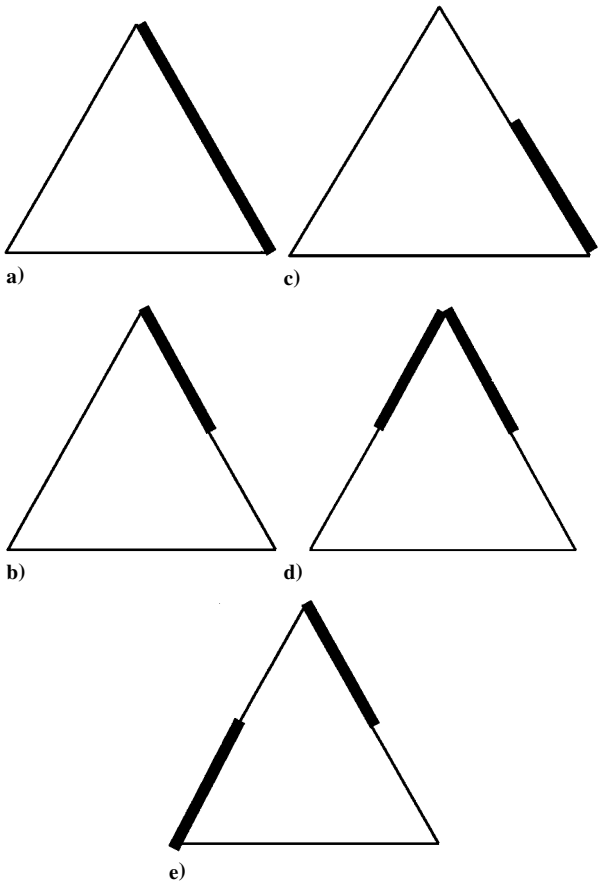

Fig. 2 Actuators: a) AT, b) forward HAT, c) rear HAT, d) two-sided HAT for pitching control, and e) two-sided HAT for yawing control. (Note: actuators are represented by the thicker line segments.)

altered by the use of microactuators and how an unbalanced vortex pair can be used to generate appreciable torques at high AOAs.

Experimental Setup and Procedures

A delta wing model with a sweep angle of 56.5 deg was sting mounted in a 0.9×0.9 m^2 low-speed wind tunnel. The model support rig has a pitch angle range of -5 to 40 deg, resulting in a 45-deg range in AOA. The wing has a constant thickness of 1.27 cm ($\sim$4.23% of the root chord) with a circular leading-edge profile (Fig. 3). The maximum wind-tunnel blockage ratio is $\sim$5%, and no correction of the blockage effect was applied. Seven rows of pressure-measuring sections, distributed uniformly between 30% and 90% chord locations, were selected to provide upper-surface pressure measurements. The lower-surface pressure distribution was obtained by inverting the wing. At each row of the pressure-measuring section, there were 18 pressure taps along the half-span, including three taps located on the circular surface of the leading edge. Each pressure tap was connected to a commercially available solid-state gauge pressure sensor (NPC-1210, Lucas NovaSensor) to map out the pressure distribution. Test Reynolds numbers range from 2.1×10^5 to 8.4×10^5, based on the wing root chord and the freestream velocities from 10 to 40 m/s.

A robust magnetic microelectromechanical-systems (MEMS) actuator was designed and fabricated for this study.[36,37] The surface-micromachined magnetic actuator (Fig. 3c) has two torsional support beams and has been successfully used for vortex flow control in an earlier study.[35] The actuator has a flap-type structure with an electroplated magnetic layer, which is supported by silicon nitride torsional beams. The flap can be activated under the influence of an external magnetic field. Experimental results have demonstrated that the flexural actuator can achieve a vertical displacement of 2 mm (at a deflection angle of 90 deg) and is robust enough to withstand a high wind loading. In this work, The microactuators were

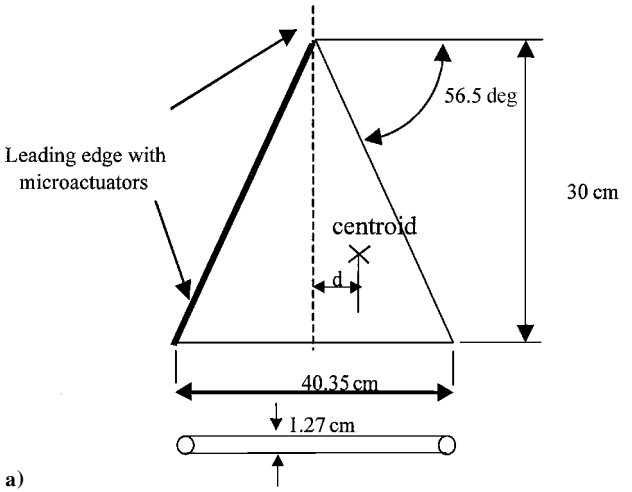

a)

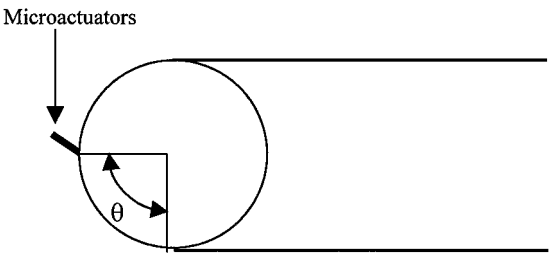

b)

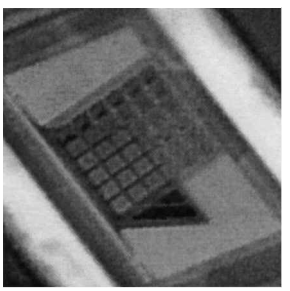

c)

Fig. 3 a) Delta wing model, b) schematic of microactuators set up on the leading edge, and c) picture of a surface-micromachined actuator.

applied on the leading-edge surface of the wing model to control the vortices. Because of the limited supply of microactuators, we also used miniature mechanical actuators for some wind-tunnel tests. Basically, the mechanical actuator has the same deflection length as the microactuators, except that the stiffness of the mechanical actuator is larger. The effects caused by using either MEMS actuators or miniature mechanical actuators were found to be comparable.

Normal force and three-axis moment data were measured by using a six-component force/moment transducer (AMTI, Inc.). This transducer system was used to record changes in torques induced by the use of microactuators. Data were digitized by an analog-to-digital converter and processed by a personal computer (PC).

Qualitative flow behaviors with and without flow control were also observed by using a laser-sheet flow visualization technique. Special attention was placed on the tracking of the movement of vortex cores under control conditions. Figure 4 shows the experimental setup for the flow visualization on the upper side of the wing model. For the flow to be visualized, a sheet of laser light (2 mm thick) from a pulsed Nd:YAG laser was projected across the wind tunnel to intercept the delta wing at any chosen chordwise location. Smoke particles generated from a stage smoke generator were used to seed the flow. The cross-flow plane of the wing was illuminated to investigate the structure of the vortices. The tests were conducted in the 0.3×0.3 m^2 low-speed wind tunnel at University of California, Los Angeles. This wind tunnel is specially designed for the purpose of flow visualization. A half-scaled wing model of the one used in 0.9×0.9 m^2 wind tunnel was used for flow visualization. Shorter 1-mm MEMS actuators were used instead of 2-mm actuators in the large wind tunnel, because of the relatively smaller size of the wing model. An image-processing system, consisting of a high-resolution charge-coupled device video camera, an image interface card, and a PC, was used for image acquisition.

Results and Discussion

Baseline Testing

First, tests were conducted without flow control to establish the baseline condition. Figures 5a and 5b represent the variation of the pressure coefficient, C_p, along the spanwise location at different cross sections at an AOA of 25 deg. For each of the measured profiles, the negative pressure distribution reaches a maximum at ~65% spanwise location. This negative peak value increases toward the wing apex and attains a maximum value of −3.5 at 30% chord location. This indicates that the leading-edge vortex has a well-defined conical structure and that the vortex core is located approximately above this spanwise position. Further downstream, the negative peak pressure regions gradually expand and their peak values decrease, signifying the downstream growth of the vortex.

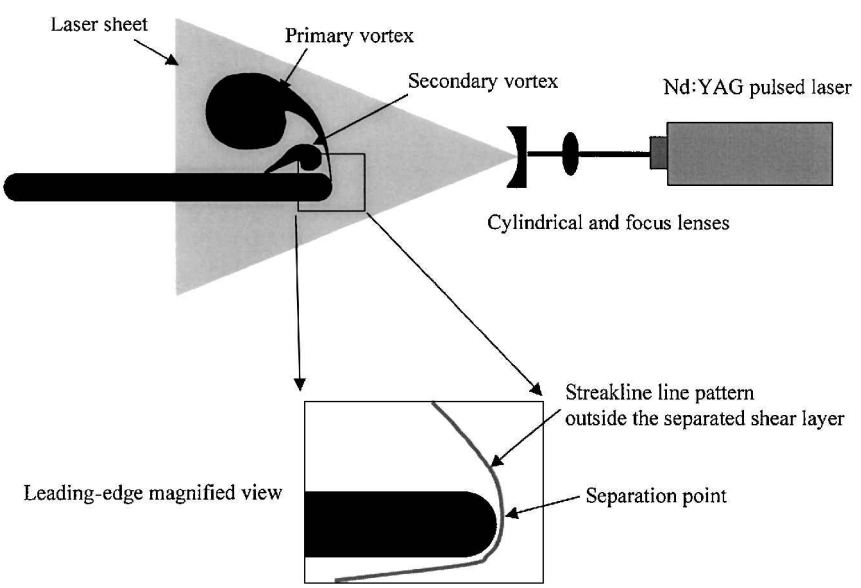

Fig. 4 Experimental setup for flow visualization.

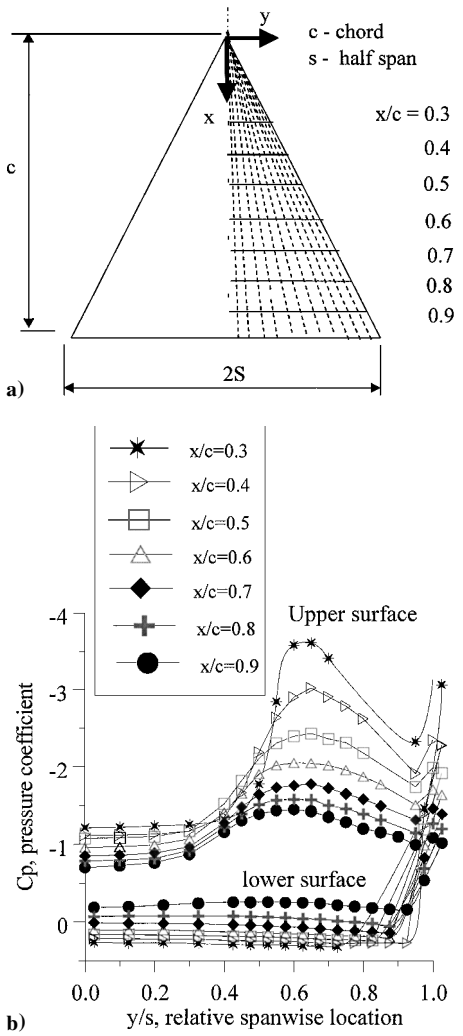

Fig. 5 a) Schematic setup for surface pressure measurements for a delta wing and b) pressure distributions of a delta wing at AOA = 25 deg.

However, the negative pressure peak at each chordwise location still remains close to 65% spanwise location. Although not presented here, similar pressure distributions were also measured at several other AOAs; ranging from 5 deg to 35 deg. By integrating the pressure distributions on both the upper and lower surfaces of a delta wing, one can obtain the total normal force acting on the wing. Note that pressure distributions near the apex were extrapolated from the measured data based on the conical vortex structure assumption. Figure 6a shows the results of the integrated pressure force at different AOAs. The normal force increases with AOA until it reaches a maximum value at an AOA of 30 deg. When this was compared with data obtained from the six-component transducer system, it was found that the difference was within 3% for each case. This confirms the reliability of the aerodynamic loading data obtained by integrating the surface pressure distributions.

Apex–Trailing Edge Microactuators

The previous study[34] has shown that rolling and pitching moments could be generated by activating a linearly distributed array of AT microactuators at strategic locations. Figures 6b and 6c show the increased rolling and pitching moments obtained from integrating the surface pressure field, while AT actuators were activated at different Reynolds numbers. The rolling and pitching moments obtained from the six-component transducer are also plotted on the same figures for comparison. In order to characterize the effectiveness of the vortex control on the wing's maneuverability, the torques measured either from the six-component transducer or from the surface pressure integration were normalized by a reference torque, which is defined as the estimated magnitude of the torque generated

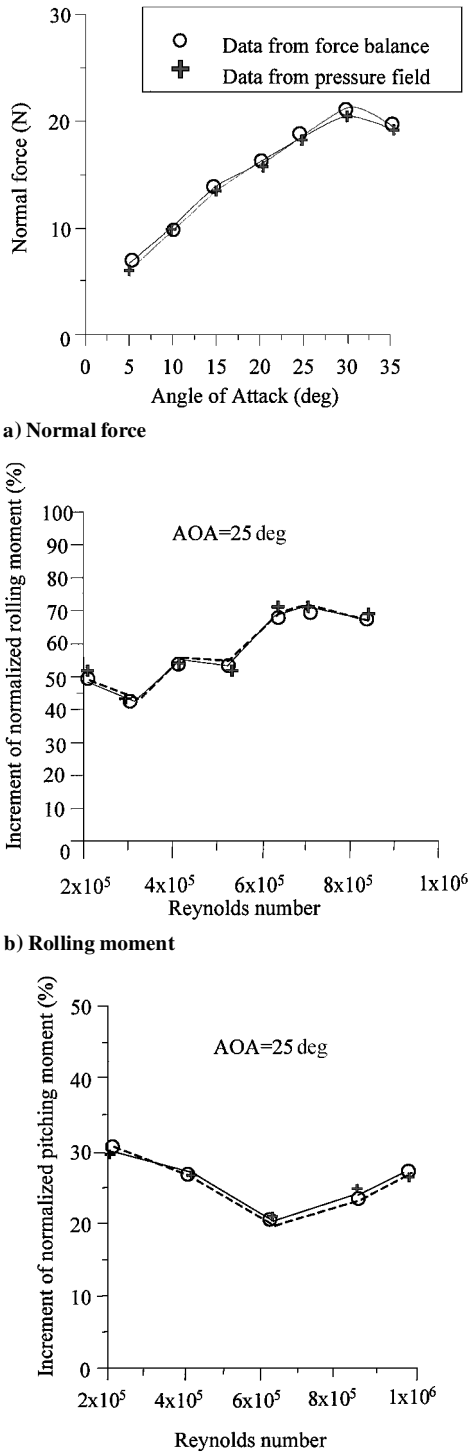

Fig. 6 Comparison of the normal force from surface pressure measurements and a six-component sensor.

by a single vortex. The procedures used for the normalization of the torque data are described as follows. First, the magnitude of vortex lift (L_v) at a specific AOA is calculated from theoretical prediction.[9] The theoretical formula has been verified by experimental data for vortical flow before vortex breakdown occurs. Then, the reference torque produced by this vortex is defined by multiplying this vortex lift to a characteristic length (d), which is chosen as the distance from the centerline of the whole wing to the centroid of a half-wing (Fig. 3). The reference torque represents the nominal capability of a single leading-edge vortex to produce torque on a delta wing, and it can be used as a standard to measure the relative magnitude of the torque generated by using the actuators. In this paper, all changes

of the three-axis torques were normalized by this reference torque for easy comparison.

Data in Fig. 6b show the change of normalized rolling moment as a function of the Reynolds number. An approximately 70% increase of normalized rolling moment can be achieved for a Reynolds numbers higher than 6×10^5. It is believed that the microactuators become increasingly more effective because the leading-edge boundary layers are thinner at higher Reynolds number cases. For pitching moment generation as shown in Fig. 6c, the increment of normalized pitching moment also shows slight dependence on the Reynolds number. An approximately 30% increase in pitching moment can be achieved at a Reynolds number of 2×10^5. Data from integration of the surface pressure field are consistent with those measured by using the six-component transducer. The maximum difference between data measured by these two methods is less than 5% for all cases.

The data from six-component transducers were also converted into moment coefficients as shown in Fig. 7. The pitching, yawing, and rolling moment coefficients are defined, respectively, as

$$C_m = \Delta M_m / q_\infty A_s \underline{c} \tag{1}$$

$$C_n = \frac{\Delta M_n}{2 q_\infty A_S S} \tag{2}$$

$$C_l = \frac{\Delta M_l}{2 q_\infty A_S S} \tag{3}$$

where ΔM_m, ΔM_n, and ΔM_l are changes in the pitching, yawing, and rolling moments induced by microactuators; q_∞, A_s, and C are the dynamic pressure of the freestream, the wing area, and the distance measured between the apex and the centroid of the wing. The maximum pitching and rolling moment coefficients are 0.025 and 0.028, respectively. However, the maximum value of the yawing moment coefficient is measured to be only 0.0043.

Half-Apex to Trailing Edge Microactuators

In a previous study,[35] an AT actuator array (Fig. 2a), covering the whole leading edge from the apex to the trailing edge, was used to successfully generate torques for flight control. In addition, it was also shown that two-leading edge vortices appeared to act independently when they were under external control. In the present case, a shorter actuator array covering only half of the leading edge, called the HAT actuator (Figs. 2b and 2c), was used to explore the possibility of more effective torque generation. Also, two HAT actuator arrays (called two-sided HAT actuators, as shown in Figs. 2d and 2e) were placed along each side of the leading edge of the wing in order to control the two leading-edge vortices individually, hence increasing the control capability.

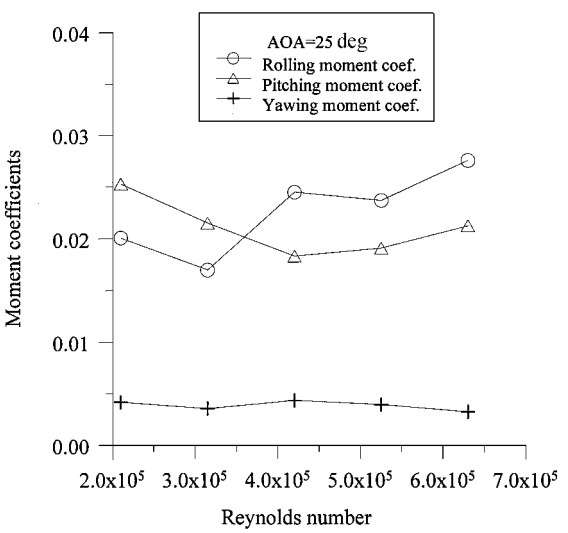

Fig. 7 Maximum rolling, pitching, and yawing moment coefficients at AOA = 25 deg.

Rolling Moment

From a previous study,[35] it has been shown that the normalized rolling moment can be increased up to a maximum of ±35% by using a linearly distributed array of 2-mm AT actuators (Fig. 8). The variation of the rolling moment is plotted as a function of the angular position (as defined in Fig. 3) of the actuator array for different Reynolds numbers. A positive peak is generated when the actuator array is placed at an angle between 40 deg and 50 deg, whereas a negative peak appears when the actuator is located at an angle of 80 deg. In the current study, we concentrated on investigating the use of the HAT actuator for more effective torque generation. Initially, a single HAT actuator was placed at the forward half of one side of the leading edge at an AOA of 25 deg (as shown in Fig. 2b). Figures 9–11 show the changes of normalized rolling, pitching, and yawing moments when HAT actuators are placed at different angular locations, respectively. Somewhat surprisingly, the maximum increase of the positive rolling moment (55% at a 60-deg angle) obtained under this control condition (Fig. 9) was found to be much higher than the increased value (35%) obtained by using the AT actuator array (Fig. 8). In contrast, the maximum increase of the negative rolling moment is not as high relative to that generated by

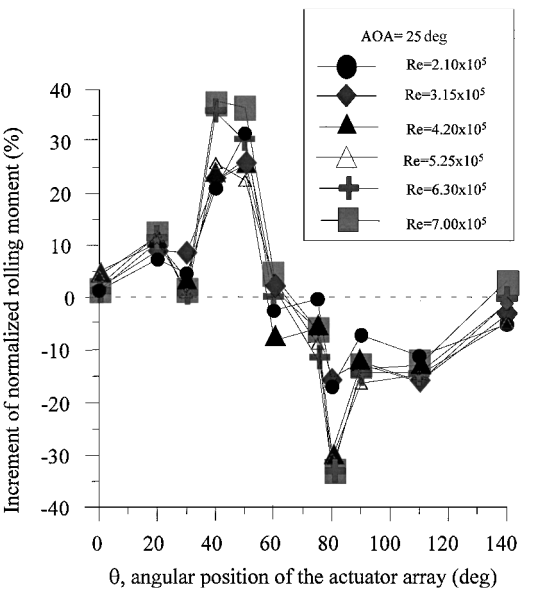

Fig. 8 Normalized rolling moment vs actuation locations at AOA = 25 deg for AT actuators.

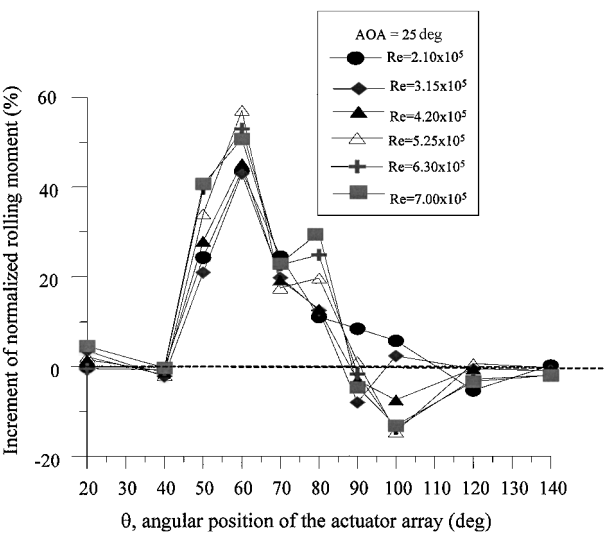

Fig. 9 Normalized rolling moment vs actuator location at AOA = 25 deg for forward HAT actuators.

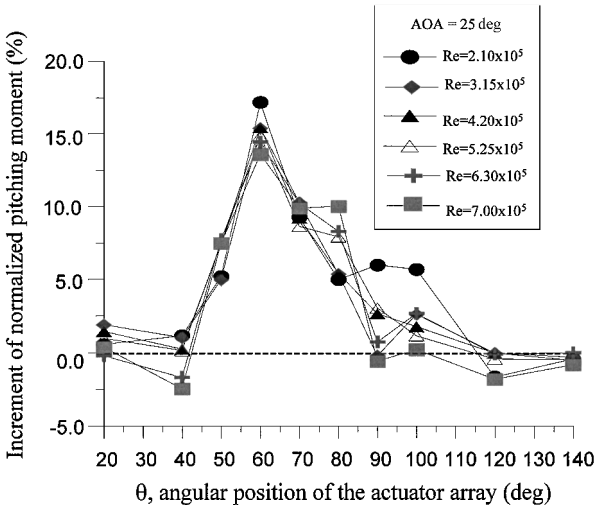

Fig. 10 Normalized pitching moment vs actuator location at AOA = 25 deg for forward HAT actuators.

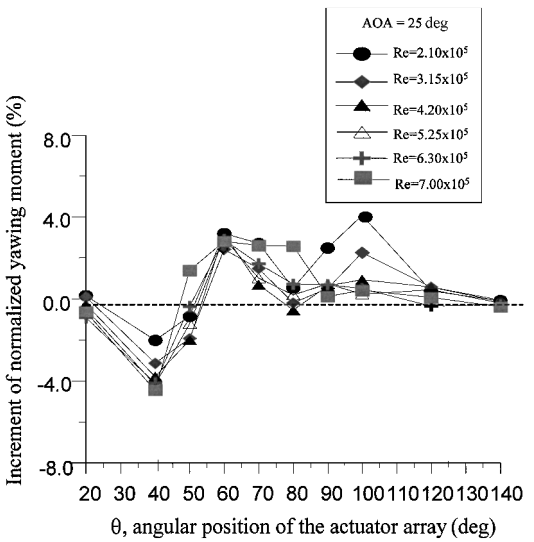

Fig. 11 Normalized yawing moment vs actuator location at AOA = 25 deg for forward HAT actuators.

using an AT actuator array (−15% at a 100-deg angle as compared with −35%). This might be because the separation line is not straight along the leading edge and the vortical flow in different sections responds differently to the local actuator array. In order to examine this possibility, we measured the separation line (from apex to trailing edge of the wing) by using distributed micromachined shear-stress sensors,[34] and the result is shown in Fig. 12. The micromachined shear-stress sensor array is a thermal-type sensor that relates the convective heat loss of an electrically heated sensor to the local surface shear stress. It has been applied successfully in the detection of boundary-layer separation.[34] It is noticed that the optimum angular position of the HAT actuator where the maximum rolling moment is produced ($\theta = 60$ deg) is very close to the measured separation line on the forward half of the leading edge. This is reasonable, as microactuators should be most effective when placed close to the separation line, where the separating boundary layer is most susceptible to external perturbations. In contrast, an AT actuator array that spans the whole length of the leading edge cannot closely match the entire separation line. Consequently there might be some adverse effects caused by this mismatch, and the use of a full AT actuator can actually reduce the overall control. Further investigation concerning the effect of the actuator array on the rear half of the wing was also undertaken by placing a HAT actuator at the rear half of the wing as shown in Fig. 2c. It was found that the rear-half HAT actuator

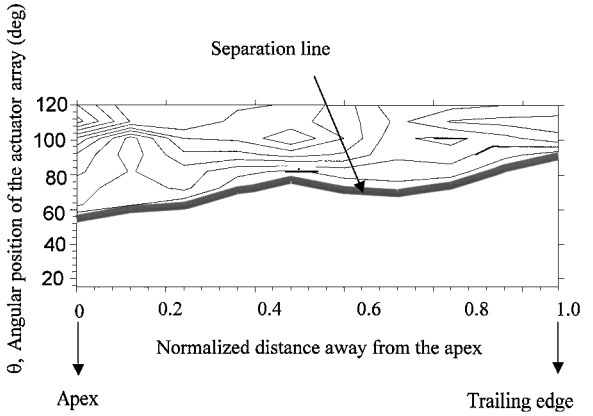

Fig. 12 Boundary-layer separation line along the wing's leading edge, determined with distributed shear-stress sensors at AOA = 25 deg ($Re = 6 \times 10^5$). The contour lines indicate the constant value of shear stress and the thicker line represents the location where flow starts to separate.

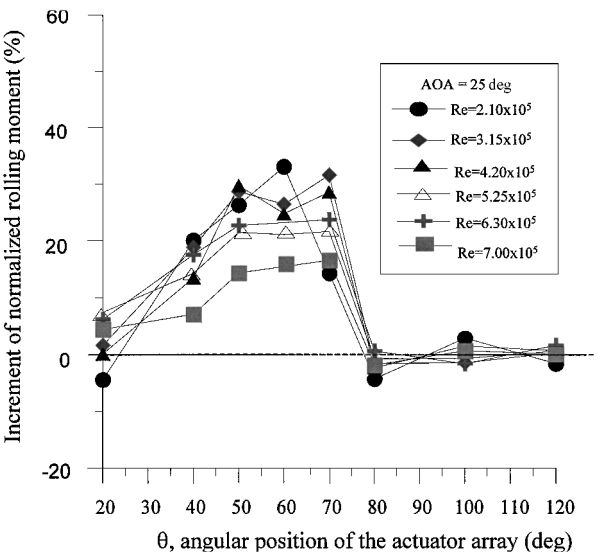

Fig. 13 Normalized rolling moment vs actuator location at AOA = 25 deg for rear HAT actuators.

array case was not as effective in generating rolling moment as the forward-half case (Fig. 13 as compared with Fig. 9). The maximum increase of the rolling moment is only ~30% or lower, and it occurs at an angle of 60 deg; close to the optimum angle for the forward HAT case. It is speculated that the rear HAT actuator cannot follow closely the rear half of the separation line because it curves inward toward the upper surface of the wing more as compared with the separation line in the forward section (Fig. 12). Moreover, it takes time for the vorticity of the separated shear layer to roll into a vortex, and perturbations generated at the leading edge will only affect the region further downstream of the wing section. Therefore, the vortex control is more effective when the actuator is placed close to the apex of the wing. This is consistent with the fact that most of the vorticity within the leading-edge vortex actually originates near the apex of the wing. Another interesting observation is that the rear actuator array does not generate negative rolling moment (Fig. 13).

Pitching and Yawing Moments

In addition to the rolling moment, pitching and yawing moments can also be induced by manipulating the leading-edge vortex pair. The generation of pitching and yawing moments could be explained by the redistribution of surface pressure field caused by microactuators, which will be discussed in detail in the next section. When a single HAT actuator is placed at the forward half of the wing, a maximum peak of 15% for pitching moment (Fig. 10) and 4% to −4% for yawing moment (Fig. 11) can be achieved. For the forward HAT

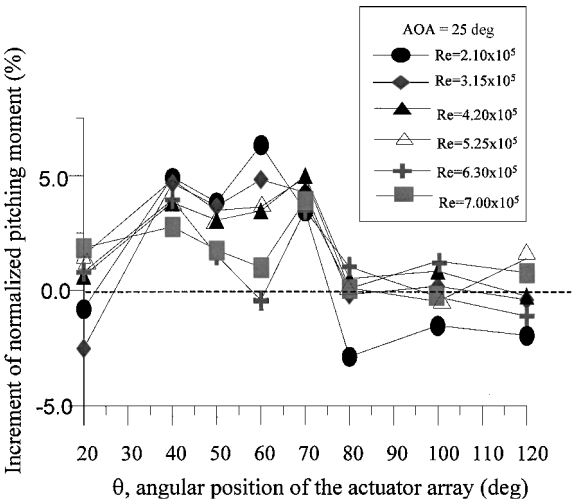

Fig. 14 Normalized pitching moment vs actuator location at AOA = 25 deg for rear HAT actuators.

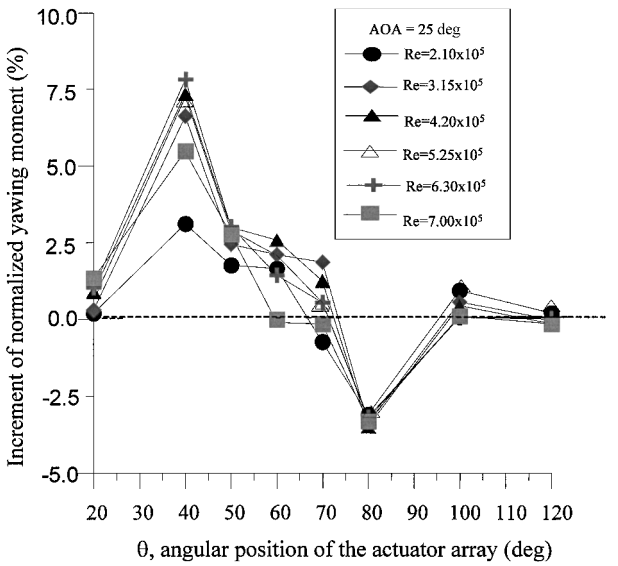

Fig. 15 Normalized yawing moment vs actuator location at AOA = 25 deg for rear HAT actuators.

actuators, the most effective angular positions for the pitching and the yawing control are different. The optimum angle is $\theta = 60$ deg for the pitching moment and $\theta = 40$ deg for the yawing moment. Furthermore, when the results were compared for the forward and rear HAT actuators, the forward HAT actuator was found to be more effective for pitching moment control (15% in Fig. 10 as compared with 5% in Fig. 14), whereas the rear HAT actuator was more effective for yawing moment control (4% in Fig. 11 as compared with 7.5% in Fig. 15).

Two-Sided HAT Actuators

In an earlier study, it was demonstrated that the two leading-edge vortices could be controlled independently.[34] Taking advantage of this behavior, we find it possible to obtain additional rolling moment if we can simultaneously activate two HAT actuator arrays located on both sides of the leading edges of the wing. For example, for a wing at an AOA of 25 deg; we can place one HAT actuator array at a 60-deg angle on one leading edge and place the other array at a 100-deg angle on the opposite side of the wing (Fig. 2d). As a result, a total rolling moment increase of 70% can be achieved if two HAT actuators are activated simultaneously at both leading edges.[34]

Another major objective of this work is to investigate the possibility of controlling pitching, rolling, and yawing moments independently by using microactuators. As shown in Figs. 9–11, all three

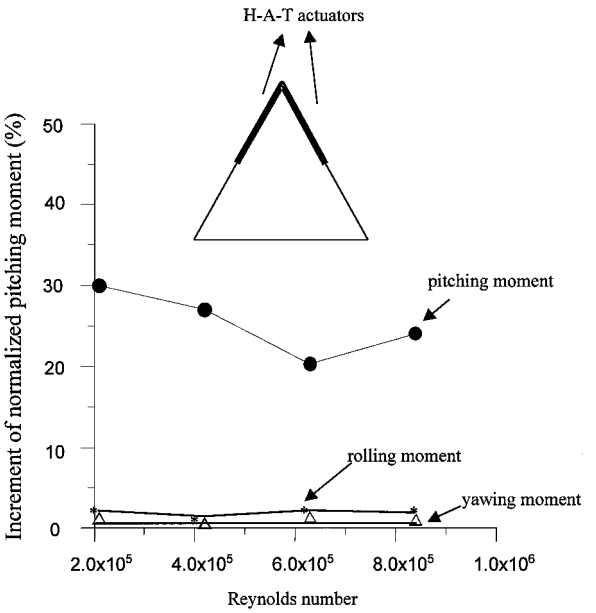

Fig. 16 Normalized pitching moment vs Reynolds number at AOA = 25 deg. Actuators are located at $\theta = 60$ deg.

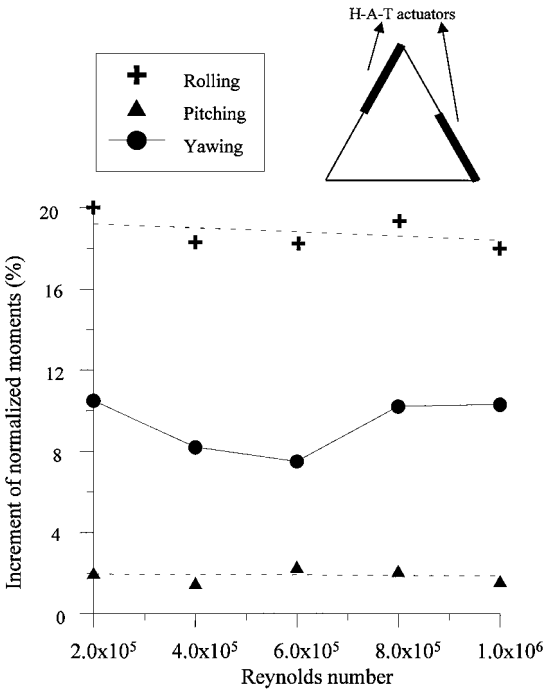

Fig. 17 Normalized yawing moment vs Reynolds number at AOA = 25 deg, two-sided HAT actuators.

moments are produced at the same time when the actuator array is activated on only one side of the leading edge. Based on simple geometric consideration, the rolling moment is produced by the emergence of an asymmetric vortex pair with respect to the wing's centerline. This implies that we can eliminate the rolling moment by activating two symmetrically located actuator arrays. As shown in Fig. 16, a maximum of 30% pitching moment can be generated by this configuration without the production of appreciable rolling (<2.8%) and yawing (<1.5%) moments. This test suggests that it is possible to provide pitching moment without generating rolling and yawing moments. A similar attempt was made to provide the maximum yawing moment by using the two-sided control configuration as shown in Fig. 2e. A yawing moment of the order of 10% could be generated without inducing significant pitching moment change (<2%). However, we could not avoid the generation of notable rolling moments (~20%) by using this configuration (Fig. 17).

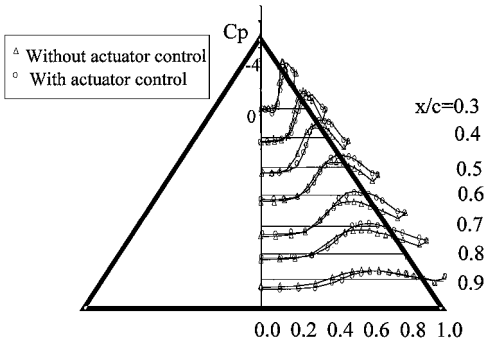

a) Positive rolling moment

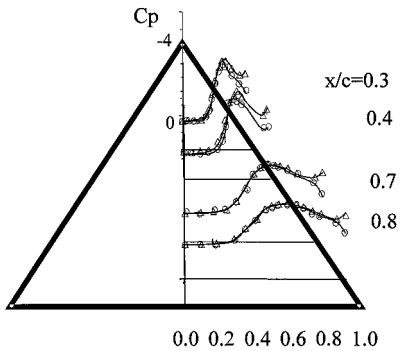

b) Negative rolling moment

Fig. 18 Surface pressure distribution on the upper side of the wing for actuators: a) before and b) downstream of the separation line.

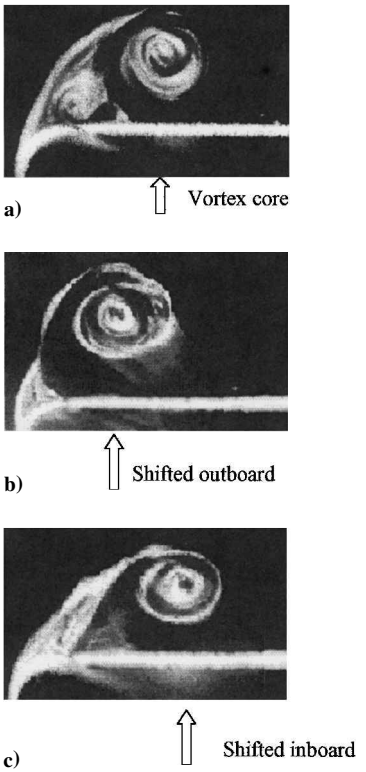

Fig. 19 Vortical structure: a) without microactuators, b) with actuators at θ = 50 deg, and c) at θ = 100 deg.

Mechanisms for Torque Generation

The rolling moment can be generated by two possible mechanisms. The first possibility is that the global structure of the leading-edge vortex is distorted such that an asymmetrically distributed vortex pair is generated. However, it is also possible that the relative strength of the two vortices has been altered by the actuators. Figure 18 shows the surface pressure fields at several cross sections on the left-hand side of the wing with and without actuation control. The distortion of the global vortex structure can be observed by surface pressure measurements. The results indicate that, on one hand, if the microactuator array is placed upstream of the separation point, it can move the peak of the surface pressure distributions outboard (Fig. 18a), generating a positive rolling moment mainly as a result of an increase of the moment arm with respect to the centerline. On the other hand, the activation of microactuators downstream of the separation point moves the peak of the surface pressure distributions inboard (Fig. 18b), and a negative rolling moment is generated as the moment arm is shortened. From both the integration of the surface pressure field and the direct force measurement data, the normal force of the wing does not show any appreciable change when microactuators were activated on only one side of the delta wing. This seems to suggest that the overall strength of the vortex system has not been changed drastically under control.

From our measurements, the maximum positive peak rolling moment emerged when the actuator array was placed at an angular position of 60 deg, whereas the maximum negative rolling moment took place when the actuator array was located at 100 deg (Fig. 9). It was expected that the most dramatic changes would occur at these angles; therefore, they were chosen to investigate the effects of microactuators' positions on vortex structures. Figure 19 shows a sequence of three flow visualization pictures corresponding, respectively, to the leading-edge vortex without control and with actuator control placed at two different angular positions. All three pictures were taken at the same chordwise location, which was 30% chord downstream of the apex where vortex breakdown had not yet occurred. Figure 19a shows the right-sided leading-edge vortex with no control, and it clearly reveals that a pair of counter-rotating stationary vortices lies on the leeward side of the wing. One can see the shear layer separating from the leading edge and rolling into a large vortex, the primary vortex. The primary vortex reattaches to the surface but separates again as the attached flow moves outboard. This leads to the emergence of the secondary vortex, as can be clearly seen underneath the separating shear layer. When the location of the vortex core was measured carefully from the picture, it was found that the vortex core was located at an ~65% spanwise location for a wing at an AOA of 25 deg. This result is consistent with the surface pressure measurements (Fig. 18).

The corresponding vortex structure when an array of forward HAT actuators is activated at $\theta = 60$ deg is shown in the following picture (Fig. 19b). It can be clearly seen that the core of the vortex has moved outboard relative to the uncontrolled vortex. This observation is concordant with the result from the surface pressure measurements. It is also evident that the shear layer separates from the leading edge with a steeper angle. It seems that the effect of the microactuators is to push the shear layer "away" from the surface. Because at this angular position the microactuators are placed ahead of the original separation point, the flow is forced to separate earlier as a result of the higher pressure gradient caused by the presence of the microactuator. Consequently, the separation vortex moves outboard and a positive rolling moment is generated because the vortex pair is unbalanced. Finally, the controlled case appears to have a larger primary vortex and a smaller secondary vortex as compared with the case of the wing without control. From both the direct force and the surface pressure measurements, the strength of the displaced primary vortex does not seem to increase drastically. It is believed that the vortex is simply becoming more diffuse rather than being strengthened.

Figure 19c shows the flow visualization result of the vortex when a HAT actuator is activated at $\theta = 100$ deg. Also consistent with the data from surface pressure measurements, the core of the vortex under this mode of actuation control has shifted inboard relative to an uncontrolled vortex. It is also noticed that the shear layer now separates from the leading edge with a smaller angle. It appears that the microactuators tend to pull the separating shear layer "toward" the wing's surface. One possible mechanism is explained as follows. When the flap actuator extends away from the surface downstream

of the original separation point, it actually reduces the effective curvature experienced by the local flow such that the adverse pressure gradient is alleviated. As a result, the flow follows the surface longer and the separation is delayed. It is expected that the boundary layer eventually separates from the surface and reattaches to the extended tip of the actuator array, where it experiences a stronger inward flow stream and, consequently, the separated layer is pulled further inward and the resulting vortex also moves inboard. A negative rolling moment is therefore generated. The vortex appears to be smaller but closer to the surface. As a result, the pressure field induced by the vortex does not change significantly (Fig. 18).

In the following paragraphs, we focus our visual observation on the region near the leading edges of the delta wing, where the interaction between the microactuators and the separated flow is the most critical to ensure an effective flow control. Our objective is to identify the relationship between the leading-edge separation pattern and the position of the actuator array.

Figure 20 shows the vortical flow patterns near the leading edge corresponding to the same configurations as shown in Fig. 19. Our interpretations of the behavior of the vortex under different control conditions are illustrated schematically next to the corresponding flow visualization pictures. Without control, the flow accelerates near the leading edge and separates as a result of the presence of an adverse pressure gradient further downstream. From this picture (Fig. 20a), the boundary-layer flow separates at ~60 deg. If an array of actuators is used before the separation line at $\theta = 50$ deg, it is found that the flow separates earlier and the deflection angle of the shear layer after separation is changed (Fig. 20b). Because of the presence of the microactuators, the boundary layer is forced to separate from the tip of the actuator array and the separated shear layer is pushed away from the surface. The flow at this location tends to carry the shear layer further outward and, consequently, the deflection angle of the shear layer is larger than that in the case without any actuation. As a result, the vortex structure is moved outboard, as has also been discussed before (Fig. 19b). Accordingly, the suction pressure peak associated with the vortex also moved outboard and a positive rolling moment was generated by the unbalanced vortex pair.

In contrast, when the actuators were placed at $\theta = 100$ deg, downstream of the uncontrolled separation position, a different trend was observed; the results were as shown in Fig. 20c. The separated boundary layer seems to attach back to the extended tip of the actuator. The effective local curvature near the actuator tip is much smaller than that without the flap. Consequently, the outflow tends to turn more sharply toward the surface of the wing so that it carries the shear layer further inward. As a result, the deflection angle of the shear layer becomes smaller and the vortex structure is moved inboard (Fig. 19c). This is consistent with the results presented in the previous sections. Consequently, a negative rolling moment is created.

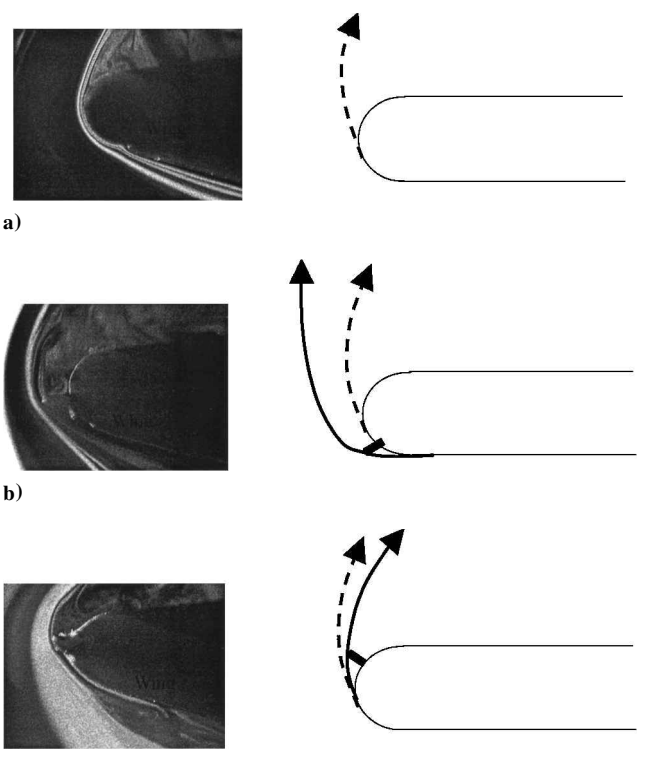

Fig. 20 Streakline flow pattern near the leading edge: a) without any actuator, b) with actuators before the original separation line, and c) with actuators downstream of the original separation line. Dashed lines indicate the original streamlines; solid lines represent separating streamlines under control.

Conclusions

A pair of nearly symmetric vortices separating from the leading edge characterizes the flow over a delta wing. At high angles of attack, these vortices make a significant contribution to the total lift of the wing. Hence, if the symmetry of these vortices can be broken by using microactuators, it is possible to generate appreciable moments for flight control. A linearly distributed array of MEMS actuators was applied in a previous study[31] to generate torques for flight control successfully. In this study, a HAT actuator covering only half the length from the apex to the trailing edge was used to explore the possibility of providing robust vortex control. It was found that a higher rolling moment could be obtained by activating an array of HAT microactuators at an appropriate location, because it could be aligned more closely to the separation line. Two-sided HAT actuator arrays were also tested to increase the control capability. Data showed that the pitching moment could be generated independently without rolling and yawing moments by applying symmetric actuation on both sides of the wing. A laser-sheet flow visualization of the delta wing flowfield was used to examine the interaction between microactuators and the cross-flow patterns of the separated boundary layer near the leading edge. Special attention was focused on the identification of the distortion of the vortex structure, particularly the movement of the vortex core, under the influence of the actuation control. It was found that the shear layer separated with a steeper angle if the actuator array was placed at or before the original separation point; hence, the vortex moved outboard and away from the surface, generating a positive rolling moment. In contrast, the shear layer separated with a smaller angle if the actuator array was positioned downstream of the original separation point. This type of control forced the vortex to move inboard and closer to the surface, producing a negative rolling moment. These flow visualization observations are consistent with data obtained by using surface pressure and direct force measurements.

Acknowledgments

This work was supported by the Defense Advanced Research Projects Agency, Microsystem Technology Office (MTO) and managed by the U.S. Air Force Office of Scientific Research. The authors thank John Seymour for his assistance in assembling the experimental setup.

References

[1]Ericsson, L. E., and Reding, J. P., "Approximate Nonlinear Slender Wing Aerodynamics," *Journal of Aircraft*, Vol. 14, No. 12, 1977, pp. 1197–1204.

[2]Payne, F. M., Ng, T. T., and Nelson, R. C., "Visualization and Wake Surveys of Vortical Flow over a Delta Wing," *AIAA Journal*, Vol. 26, No. 2, 1988, pp. 137–143.

[3]Fink, P. T., and Taylor, J., "Some Early Experiments on Vortex Separation," Aeronautical Research Council, Repts. and Memoranda 3489, Sept. 1966.

[4]Lambourne, N. C., and Bryer, D. W., "The Bursting of Leading-Edge Vortices—Some Observations and Discussion of the Phenomenon," Aeronautical Research Council, Repts. and Memoranda 3282, April 1961, pp. 1–37.

[5]Lee, M., and Ho, C. M., "Lift Force of Delta Wings," *Applied Mechanics Review*, Vol. 43, No. 9, 1990, pp. 209–221.

[6]Peckham, D. H., "Low-Speed Wind-Tunnel Tests on a Series of Uncam-

bered Slender Pointed Wings with Sharp Edges," Aeronautical Research Council, Repts. and Memoranda 3186, Dec. 1958.

[7]Earnshaw, P. B., and Lawford, J. A., "Low-Speed Wind-Tunnel Experiments on a Series of Sharp Leading-edged Delta Wings," Aeronautical Research Council, Repts. and Memoranda 3424, Jan. 1966.

[8]Hall, M. G., "Vortex Breakdown," *Annual Review of Fluid Mechanics*, Vol. 4, No. 8023, 1972, pp. 195–218.

[9]Polhamus, E. C., "Predictions of Vortex-Lift Characteristics by a Leading-Edge Suction Analogy," *Journal of Aircraft*, Vol. 8, No. 4, 1971, pp. 193–199.

[10]Bradley, R. G., and Wray, W. O., "A Conceptual Study of Leading-Edge-Vortex Enhancement by Blowing," *Journal of Aircraft*, Vol. 11, No. 1, 1974, pp. 33–38.

[11]Wood, N. J., and Roberts, L., "The Control of Vortical Lift on Delta Wings by Tangential Leading Edge Blowing," AIAA Paper 87-0158, Jan. 1987.

[12]Campbell, J. F., "Augmentation of Vortex Lift by Spanwise Blowing," *Journal of Aircraft*, Vol. 13, No. 9, 1976, pp. 727–732.

[13]Greenwell, D. I., and Wood, N. J., "Roll Moment Characteristics of Asymmetric Tangential Leading-Edge Blowing on a Delta Wing," *Journal of Aircraft*, Vol. 31, No. 1, 1994, pp. 161–168.

[14]Johari, H., Olinger, D. J., and Fitzpatrick, K. C., "Delta Wing Vortex Control via Recessed Angled Spanwise Blowing," *Journal of Aircraft*, Vol. 32, No. 4, 1995, pp. 804–810.

[15]Gu, W., Robinson, O., and Rockwell, D., "Control of Vortices on a Delta Wing by Leading-Edge Injection," *AIAA Journal*, Vol. 31, No. 7, 1993, pp. 1177–1186.

[16]Miyaji, K., Fujii, K., and Karashima, K., "Enhancement of the Leading-Edge Separation Vortices by Trailing-Edge Lateral Blowing," *AIAA Journal*, Vol. 34, No. 9, 1996, pp. 1943–1945.

[17]Meyer, J., and Seginer, A., "Pulsating Spanwise Blowing on a Fighter Aircraft," AIAA Paper 92-4359, Washington, DC, 1992, pp. 188–197.

[18]Gad-el-Hak, M., and Blackwelder, R. F.,"Control of the Discrete Vortices from a Delta Wing," *AIAA Journal*, Vol. 25, No. 8, 1987, pp. 1024–1049.

[19]Celik, Z. Z., and Roberts, L., "Aircraft Control at High-Alpha by Tangential Blowing," AIAA Paper 92-0021, Jan. 1992.

[20]Greenwell, D. I., and Wood, N. J., "Static Roll Moment Characteristics of Asymmetric Tangential Leading Edge Blowing on a Delta Wing at High Angles of Attack," AIAA Paper 93-0052, Jan. 1993.

[21]Fitzpatrick, K., Johari, H., and Olinger, D., "A Visual Study of Recessed Angled Spanwise Blowing Method on a Delta Wing," AIAA Paper 93-3246, July 1993.

[22]Malcom, G. N., and Skow, A. M., "Flow Visualization Study of Vortex Manipulation of Fighter Configurations at High Angles of Attack," CP-413, AGARD, 1986.

[23]Alexander, M., and Meyn, L. A., "Wind Tunnel Results of Pneumatic Forebody Vortex Control Using Rectangular Slots on a Chined Forebody," AIAA Paper 94-1854, June 1994.

[24]Hummel, D., "Zur Umstromung Sharfkantiger Shlanker Deltaflugel bei Grossen Anstellwinkeln," *Zeitschrift fuer Flugwissenschaften*, Vol. 15, No. 10, 1967, pp. 376–385.

[25]Ross, F. W., and Kegelman, J. T., "Recent Explorations of Leading Edge Vortex Flowfields," NASA CP-3149, Vol. 1, Pt. 1, Oct. 1990, pp. 157–172.

[26]Shih, C., and Ding, Z., "Trailing-Edge Jet Control of Leading-Edge Vortices of a Delta Wing," *AIAA Journal*, Vol. 34, No. 7, 1996, pp. 1447–1457.

[27]Helin, H. E., and Watry, C. W., "Effects of Trailing-Edge Jet Entrainment on Delta Wing Vortices," *AIAA Journal*, Vol. 32, No. 4, April 1994, pp. 802–804.

[28]Wahls, R. A., Vess, R. J., and Moskovitz, C. A., "Experimental Investigation of Apex Fence Flaps on Delta Wings," *Journal of Aircraft*, Vol. 23, No. 10, 1986, pp. 789–797.

[29]Marchman, J. F., "Aerodynamics of Inverted Leading-Edge Flaps on Delta Wings," *Journal of Aircraft*, Vol. 18, No. 12, 1981, pp. 1051–1056.

[30]Rao, D. M., and Buter, T. A., "Experimental and Computational Studies of a Delta Wing Apex-Flap," AIAA Paper 83-1815, July 1983.

[31]Rao, D. M., and Johnson, T. D. Jr., "Investigation of Delta Wing Leading-Edge Devices," *AIAA Journal*, Vol. 18, No. 3, 1981, pp. 161–167.

[32]Spedding, G. R., Maxworthy, T., and Rignot, E., "Unsteady Vortex Flows over Delta Wings," *Proceedings of the AFOSR Workshop on Unsteady and Separated Flows*, Airforce Office of Scientific Research, Colorado Springs, CO, 1987.

[33]Marchman, J. F., "Effect of Heating on Leading Edge Vortices in Subsonic Flow," *Journal of Aircraft*, Vol. 12, No. 2, 1975, pp. 121–123.

[34]Lee, G. B., "Control of a Delta-Wing Aircraft by Using Micromachined Sensors and Actuators," Ph.D. Dissertation, Dept. of Mechanical and Aerospace Engineering, Univ. of California, Los Angeles, CA, 1998.

[35]Lee, G. B., Jiang, F., Tsao, T., Tai, Y. C., and Ho, C. M., "Macro Aerodynamics Devices Controlled by Micro Systems," Institute of Electrical and Electronics Engineers, Aerospace Conf., Wazf, Feb. 1997.

[36]Ho, C. M., and Tai, Y. C. "Micro-electro-mechanical-systems (MEMS) and Fluid Flows," *Annual Review of Fluid Mechanics*, Vol. 30, 1998, pp. 579–612.

[37]Liu, C., Tsao, T., Tai, Y. C., and Ho, C. M., "Surface Micromachined Magnetic Actuators," *An Investigation of Micro Structures, Sensors, Actuators, Machines, and Systems*, edited by T. Higuchi and K. Ikuta, IEEE, New York, 1994, pp. 57–62.